npj | heritage science

Article

https://doi.org/10.1038/s40494-025-01738-3

Inverse analysis for dynamic characteristics of a historic Masonry Pagoda using segmental low-amplitude earthquake vibrations

Check for updates

Chayanon Hansapinyo[1], Chinnapat Buachart[1] ✉, Chana Sinsabvarodom[1], Warakorn Tantrapongsaton[1], Worathep Sae-Long[2], Suchart Limkatanyu[3], Hexin Zhang[4], Tohid Ghanbari-Ghazijahani[5] & Vanissorn Vimonsatit[5]

Historical structures are inherently prone to degradation, necessitating structural health monitoring for their preservation. This study proposes an inverse analysis methodology to determine structural dynamic properties, offering insights into fundamental behavior. The algorithm integrates Newmark's time-stepping method with the Gauss-Newton scheme for improved accuracy. Its effectiveness is demonstrated using four seismic datasets from distant earthquakes. A Historic Masonry Pagoda in Chiang Mai, Thailand, was monitored via segmental low-amplitude earthquake data. Two 3-directional vibration sensors at the top and base recorded responses during seismic events. Given the low amplitude, each 120-s event was divided into twelve segments for enhanced analysis. The results show that segmenting seismic waves increases output data, reducing uncertainties through probabilistic techniques. As the pagoda's structural properties remain partially unknown, the derived dynamic properties establish a baseline for future assessments of deterioration.

Earthquakes have the potential to inflict extensive damage upon cities. In light of the inevitability of seismic events, considerable resources have been allocated to the development of robust preparedness strategies[1,2]. Buildings of heightened significance are categorized based on the potential loss consequences, with historical structures particularly vulnerable due to outdated construction techniques lacking seismic considerations. Moreover, these buildings hold significant cultural value. Consequently, they are identified, classified as highly critical, and urgently necessitate seismic reinforcement[3].

The Northern region of Thailand is well-known for its numerous active fault lines. A significant event occurred on May 5, 2014, when a 6.3-magnitude earthquake struck Chiang Rai Province, causing widespread structural damage[4]. Due to the abundance of historical buildings in Northern Thailand, the need for immediate seismic strengthening measures is critical. To support this effort, understanding the dynamic properties of structures —such as damping ratio and fundamental period of vibration—is essential. Previous studies have indicated that ground motion, influenced by various parameters and resonance effects, may have contributed to the structural damage observed during earthquakes. Mase et al. [5] examined ground motion parameters and conducted site assessments in Northern Thailand following the Tarlay Earthquake. Their analysis focused on ground motion data recorded at the Mae Sai Station (MSAA), the nearest seismic station to the earthquake rupture[6].

Seismic phenomena in earthquakes inherently possess stochastic characteristics[7], a critical consideration in earthquake-resistant design. This significance is particularly evident in the dynamic aseismic design of high-rise buildings, large structures, and similar constructions[8,9]. Various procedures exist for designing criteria to withstand earthquakes, utilizing established methods for integrating strong ground motion records into the seismic design framework of structures. Recognizing that time history signals recorded at a site constitute a random process that is practically impossible to replicate, substantial efforts have been made in recent years to process actual records to make them "representative" of future input histories for existing and planned construction in earthquake-prone regions.

[1]Excellence Center in Infrastructure Technology and Transportation Engineering, Department of Civil Engineering, Faculty of Engineering, Chiang Mai University, Chiang Mai, Thailand. [2]Civil Engineering Program, School of Engineering, University of Phayao, Phayao, Thailand. [3]Department of Civil Engineering, Prince of Songkla University, Hat Yai, Thailand. [4]School of Engineering and the Built Environment, Edinburgh Napier University, Edinburgh, Scotland, UK. [5]School of Engineering, Macquarie University, Sydney, NSW, Australia. ✉e-mail: chinapat@eng.cmu.ac.th

This is due to the uncertainties and challenges associated with selecting earthquake records for safe design[10].

Modal analysis of fully three-dimensional finite element models has proven effective in determining dynamic properties. However, this approach is limited to buildings with available as-built drawings, making it impractical for historical structures that lack such data. In the absence of detailed information on long-standing historical buildings, modal analysis must rely on uncertain assumptions, which can lead to unrealistic results. A widely used alternative technique is the ambient vibration test, as demonstrated on the masonry roof of the Basilica of the Fourteen Holy Helpers in Bavaria, southern Germany[11], and on the Jura Chapel, in Jerez de la Frontera, Spain[12]. Operational modal analysis using this method identifies dynamic structural parameters, allowing for adjustments to numerical models to more accurately represent actual structural behavior. This approach was exemplified in the assessment of the Chapel of the Würzburg Residence in Germany[13], where modal displacements and natural frequencies were used to enhance the accuracy of the finite element model. Ambient vibration tests have also been conducted in Lebanon and Turkey[14,15], providing global vibration properties. However, the technique is limited in identifying local characteristics due to the low intensity of the vibration signal. Another common approach for estimating dynamic properties is inverse analysis, which relies on precise measurements of structural deformation during vibration, followed by mathematical analysis in reverse[16,17]. This method has been employed to assess a historical bridge in the Czech Republic[18]. However, these studies have not accounted for uncertainties arising from the randomness of earthquake vibration characteristics.

This study applies the inverse analysis method to determine the dynamic properties of a pagoda in Chiang Mai Province, Northern Thailand. Two vibration sensors, placed at the top and base of the pagoda, monitor its response during earthquake events. The resulting seismic vibrations provide robust signals for analysis. By comparing the measured ground and top accelerations with numerical results, the dynamic properties of the pagoda—specifically, the damping ratio and natural frequency—are iteratively calculated. The Gauss-Newton iteration is used to minimize the discrepancy between the measured and calculated accelerations at each time step. To solve the equation of motion, Newmark's average acceleration method is employed.

Owing to the long return period of earthquakes, the available input motions are notably limited. Distant earthquakes characterized by low signal arrivals are typically acknowledged, necessitating noise filtering. To extract more comprehensive information from individual signals, the vibration duration is subdivided into multiple 10-s intervals. This procedural refinement serves to address the inherent uncertainties in the analysis by integrating probabilistic techniques[19]. The paper likely delves into the importance of incorporating probabilistic assessments for a better understanding of dynamic properties and inverse analysis, providing valuable insights applicable to structural health monitoring and seismic damage prevention of vulnerable historical buildings.

In this paper, "Methods" presents the measurement details, mathematical formulation, and methods used in the analysis. The procedure for this present work is briefly explained in Fig. 1. First, the acceleration time history of a pagoda was measured for 4 earthquakes in both NS and EW directions. Each time history was divided into 12 segments, resulting in a total of 96 records. The inverse analysis was employed to obtain the dynamic parameters (ζ and f) from each record, followed by a statistical analysis to determine the probability distribution, mean (μ), and variance (s^2) of ζ and f. Subsequently, simulated values were derived using Newmark time integration, where dynamic parameters ζ and f are set to $\mu - 2$ s, μ, and $\mu + 2$ s. These simulated values were then compared with the measured acceleration time history. The results are provided in "Results", followed by an in-depth discussion in "Discussion".

Methods

Mathematical formulations

The mathematical formulation of a system with a single degree of freedom under the ground excitation is presented in Eq. (1):

$$m\ddot{u} + c\dot{u} + ku = -ma_g \tag{1}$$

where u, $\dot{u}$, and $\ddot{u}$ denote the relative lateral displacement, velocity, and acceleration of the structural mass, respectively. m represents the structural mass, while c and k stand for the damping coefficient and stiffness, respectively. Ground acceleration is indicated by a_g.

The stiffness (k) and damping coefficient (c) in Eq. (1) can be expressed in term of the structural mass, natural angular frequency (ω), and damping ratio (ζ) as:

$$k = m\omega^2 \tag{2}$$

$$c = 2m\omega\zeta \tag{3}$$

Substituting parameters k and c from Eqs. (2) and (3) into Eq. (1), and dividing the equation by the structural mass m, yields:

$$\ddot{u} + 2\omega\zeta\dot{u} + \omega^2 u = -a_g \tag{4}$$

Generally, for a newly constructed building or one with measurable structural properties, the dynamic properties (ω and ζ) are given. In such cases, the structural motions (u, $\dot{u}$, $\ddot{u}$) can be obtained under an induced ground motion a_g. However, for an investigation of an existing building, motions of structure and ground motion are time-domain measurements by sensors, and the dynamic properties are unknown parameters. This is especially true for historic buildings, where the central structural elements

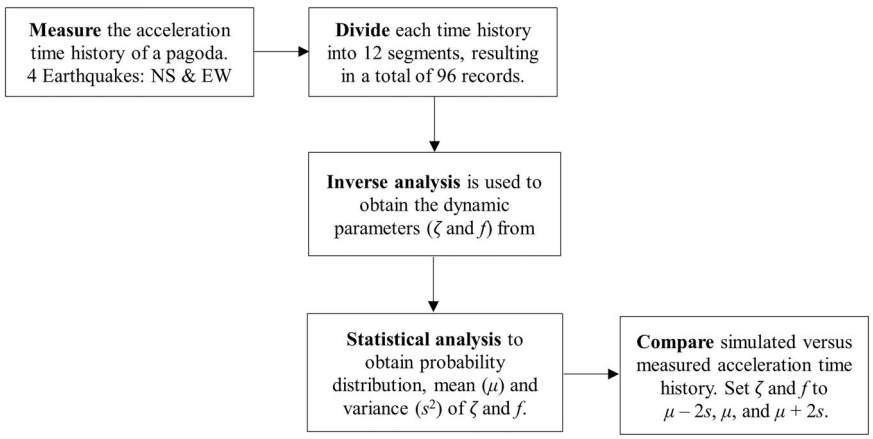

Fig. 1 | Workflow of the proposed inverse analysis method. The diagram illustrates the overall methodology: Acceleration time histories from four seismic events (in NS and EW directions) are segmented into twelve parts, resulting in 96 data segments. An inverse analysis is performed for each segment to obtain the damping ratio (ζ) and natural frequency (f). The distributions of ζ and f are then analyzed statistically to obtain their means (μ) and variances (s^2). Finally, a comparison between measured and simulated acceleration time histories is performed by applying combinations of $\mu \pm 2$ s.

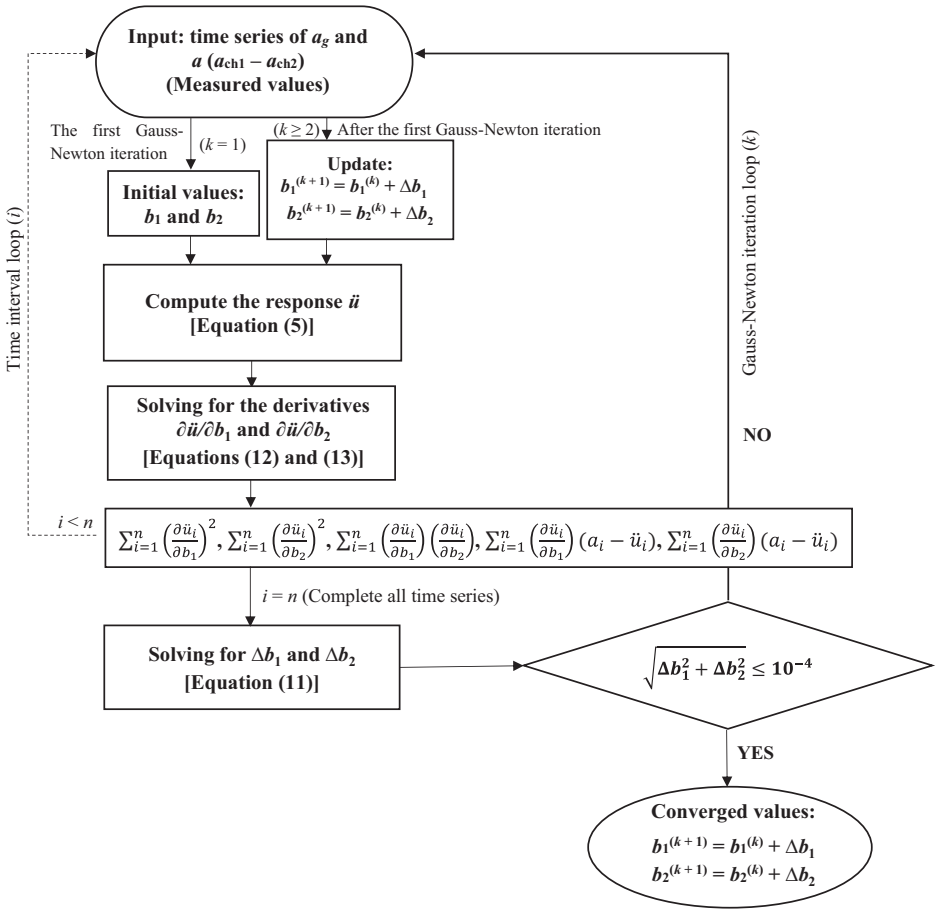

Fig. 2 | Gauss-Newton iterative procedure for updating the dynamic parameters. This flowchart presents the Gauss-Newton method used to update the parameters b_1 and b_2. Initial values are set, and response accelerations are computed based on measured ground acceleration and relative acceleration. The derivatives of acceleration with respect to each parameter are calculated. The algorithm iteratively updates the parameters until convergence is achieved, defined as the sum of squared parameters change being less than 10^{-4}. Each time interval and iteration step are shown in sequence.

may be uncertain, and any destructive investigations to determine structural properties are prohibited. In these cases, the measured motions are used for comparison with the backward-calculated motions in each time step performed in the inverse analysis by iteratively identifying the dynamic parameters, ζ and ω. The formulation of the inverse analysis is explained next.

To perform the inverse analysis, the equation of motion expressed in Eq. (4) is simplified as

$$\ddot{u} + b_1\dot{u} + b_2 u = -a_g \tag{5}$$

where $b_1 = 2\omega\zeta$ and $b_2 = \omega^2$. Solving the differential equation, the numerical time-stepping techniques are widely applied. In this study, the Newmark's time stepping scheme with average acceleration was adopted. The details of applying the numerical methods are explained in general dynamic textbooks[20,21]. As seen in Fig. 2, to determine the structural motion via the Newmark's time stepping scheme, possible ω and ζ values were first estimated, and then the parameters b_1 and b_2 were obtained. With the input ground motion a_g, the structural motions (u, $\dot{u}$, $\ddot{u}$) are numerically determined. However, the computed structural motions are not the correct ones compared with the measured values, as long as the parameters b_1 and b_2 are not correct. Hence, the process to adjust the parameters b_1 and b_2 is required, namely Gauss-Newton Method[22], which is one of the most efficient algorithm as described in[23]. First, for each time step t_i, incremental adjustments of b_1 and b_2 are introduced as

$$b_1^{(k+1)} = b_1^{(k)} + \Delta b_1^{(k+1)} \tag{6}$$

$$b_2^{(k+1)} = b_2^{(k)} + \Delta b_2^{(k+1)} \tag{7}$$

where the super-script k is the number of adjustment iteration for each time-stepping, ${b_1}^{(k+1)}$, ${b_1}^{(k)}$ and ${b_2}^{(k+1)}$, ${b_2}^{(k)}$ are the updated parameters (iteration $k+1$) and the previous parameters (iteration k), respectively. The variables $\Delta {b_1}^{(k+1)}$ and $\Delta {b_2}^{(k+1)}$ are incremental adjustment of the parameters (iteration $k+1$). Next, the difference between the computed acceleration using Eq. (5) based on the updated parameters and the measured acceleration of all time steps (n) are presented in terms of the Sum-Square-Error $SSE^{(k+1)}$, as shown in Eq. (8).

$$SSE^{(k+1)} = \sum_{i=1}^{n}\left[\ddot{u}\left({b_1}^{(k+1)}, {b_2}^{(k+1)}, t_i\right) - a(t_i)\right]^2 \tag{8}$$

where $\ddot{u}\,({b_1}^{(k+1)}, {b_2}^{(k+1)}, t_i)$ and $a\,(t_i)$ are the computed acceleration based on the updated parameters and the measured acceleration at time step t_i, respectively. $\Sigma_{i=1}^{n}$ represents the summation of the square errors from time step 1 to the end at time step n.

Mathematical expression minimizing the $SSE^{(k+1)}$ with respected to the incremental adjustments Δb_1 and Δb_2 is expressed as:

$$\frac{\partial(SSE^{(k+1)})}{\partial\Delta b_1^{(k+1)}} = 0 \text{ and } \frac{\partial(SSE^{(k+1)})}{\partial\Delta b_2^{(k+1)}} = 0 \tag{9}$$

To differentiate Eq. (9), the $SSE^{(k+1)}$ is rewritten in the form of incremental adjustments by introducing the linear approximation of the computed acceleration as

$$\ddot{u}\left({b_1}^{(k+1)}, {b_2}^{(k+1)}, t_i\right) = \ddot{u}\left({b_1}^{(k)}, {b_2}^{(k)}, t_i\right) + \Delta {b_1}^{(k+1)}\left(\frac{\partial\ddot{u}\left({b_1}^{(k)}, {b_2}^{(k)}, t_i\right)}{\partial b_1}\right) + \Delta {b_2}^{(k+1)}\left(\frac{\partial\ddot{u}\left({b_1}^{(k)}, {b_2}^{(k)}, t_i\right)}{\partial b_2}\right) \tag{10}$$

Table 1 | The pseudocode of inverse analysis procedure

Input: Time history of measured horizontal ground accelerations ($\boldsymbol{a}_g$) and pagoda acceleration ($\boldsymbol{a} = \boldsymbol{a}_{ch1} - \boldsymbol{a}_{ch2}$), and maximum number of iteration K.
Output: Approximate solution of dynamic parameters b_1 and b_2.

Initial guess for the dynamic parameters ${b_1}^{(1)}$ and ${b_2}^{(1)}$.
for $k = 1, 2, 3, \ldots, K$ **do**
Compute the pagoda responses ($\boldsymbol{u}$, $\dot{\boldsymbol{u}}$ and $\ddot{\boldsymbol{u}}$) from Eq. (5) via Newmark time integration.
Solving for the partial derivatives ($\partial\ddot{\boldsymbol{u}}/\partial b_1$ and $\partial\ddot{\boldsymbol{u}}/\partial b_2$) from Eqs. (12) and (13) via
Newmark time integration.
Solving for $\Delta {b_1}^{(k+1)}$ and $\Delta {b_2}^{(k+1)}$ from Eq. (11).
Update: ${b_1}^{(k+1)} = {b_1}^{(k)} + \Delta {b_1}^{(k+1)}$ and ${b_2}^{(k+1)} = {b_2}^{(k)} + \Delta {b_2}^{(k+1)}$
if $\sqrt{\Delta b_1^2 + \Delta b_2^2} \le 10^{-4}$ **then** exit for loop.
end of for loop
Converged values: $b_1 = {b_1}^{(k+1)}$ and $b_2 = {b_2}^{(k+1)}$

where $\ddot{u}\,({b_1}^{(k)}, {b_2}^{(k)}, t_i)$ is the computed acceleration based on the parameters at previous iteration k (i.e., ${b_1}^{(k)}$ and ${b_2}^{(k)}$), at time step t_i. For clarity, the term $\ddot{u}\,({b_1}^{(k)}, {b_2}^{(k)}, t_i)$ is shorten to $\ddot{u}_i$. Then, substituting Eq. (10) into Eq. (9) yields the Gauss-Newton equation as shown in Eq. (11), for determining the incremental adjustments $\Delta {b_1}^{(k+1)}$ and $\Delta {b_2}^{(k+1)}$.

$$\begin{bmatrix} \sum_{i=1}^{n}\left(\frac{\partial \ddot{u}_i}{\partial b_1}\right)^2 & \sum_{i=1}^{n}\left(\frac{\partial \ddot{u}_i}{\partial b_1}\cdot\frac{\partial \ddot{u}_i}{\partial b_2}\right) \\ \sum_{i=1}^{n}\left(\frac{\partial \ddot{u}_i}{\partial b_1}\cdot\frac{\partial \ddot{u}_i}{\partial b_2}\right) & \sum_{i=1}^{n}\left(\frac{\partial \ddot{u}_i}{\partial b_1}\right)^2 \end{bmatrix} \begin{Bmatrix} \Delta {b_1}^{(k+1)} \\ \Delta {b_2}^{(k+1)} \end{Bmatrix} = \begin{Bmatrix} \sum_{i=1}^{n}\frac{\partial \ddot{u}_i}{\partial b_1}\cdot\left(a_i - \ddot{u}_i\right) \\ \sum_{i=1}^{n}\frac{\partial \ddot{u}_i}{\partial b_2}\cdot\left(a_i - \ddot{u}_i\right) \end{Bmatrix} \tag{11}$$

To solve Eq. (11) for the incremental adjustments $\Delta {b_1}^{(k+1)}$ and $\Delta {b_2}^{(k+1)}$, the elements in the first matrix term of the equation are determined by taking the partial derivative of Eq. (5) with respect to parameters b_1 and b_2, resulting two second-order linear ordinary differential equations, as shown in Eqs. (12) and (13). It is noted that the change of ground acceleration is independent of the change of the dynamic parameters, hence, $\partial a_{gi}/\partial b_1$ and $\partial a_{gi}/\partial b_2$ are zero. Equations (12) and (13) resemble the equation of motion in Eq. (5), and the Newmark's time stepping scheme was adopted again to determine the terms $\partial \ddot{u}_i/\partial b_1$ and $\partial \ddot{u}_i/\partial b_2$.

$$\frac{\partial \ddot{u}_i}{\partial b_1} + b_1\frac{\partial \dot{u}_i}{\partial b_1} + b_2\frac{\partial u_i}{\partial b_1} = -\dot{u}_i \tag{12}$$

$$\frac{\partial \ddot{u}_i}{\partial b_2} + b_1\frac{\partial \dot{u}_i}{\partial b_2} + b_2\frac{\partial u_i}{\partial b_2} = -u_i \tag{13}$$

The obtained incremental adjustments $\Delta {b_1}^{(k+1)}$ and $\Delta {b_2}^{(k+1)}$ were then used for updating the dynamic parameters b_1 and b_2 as shown in Eqs. (6) and (7), then used for solving for the structural motions and errors in Eqs. (5), (6) and (7), respectively. The process iterates for calculation of the incremental adjustments until it meets a certain tolerance level as shown in Eq. (14), resulting in the converged dynamic parameters b_1 and b_2. These parameters were then used for determining the angular natural frequency (ω) or natural frequency (f), and damping ratio (ζ) through Eqs. (15) and (16). The calculation process is shown in Fig. 2.

$$\sqrt{\left(\Delta b_1\right)^2 + \left(\Delta b_2\right)^2} \le 10^{-4} \tag{14}$$

$$\zeta = \frac{b_1}{2\sqrt{b_2}} \tag{15}$$

$$\omega = \sqrt{b_2}\ \text{or}\ f = \frac{\omega}{2\pi} = \frac{\sqrt{b_2}}{2\pi} \tag{16}$$

To make clearer and more concise, the pseudocode of inverse analysis procedure (Fig. 2) is represented by Table 1.

Measurements of the Pagoda

The pagoda, located within Umong Temple (as shown in Fig. 3), is situated west of Chiang Mai City in Northern Thailand, at coordinates 18.78317°N, 98.95133°E. This study involves conducting vibration measurements on the structure. Built in 1297 by King Mengrai, the pagoda features a circular cross-sectional design, with a base diameter of 16.48 m that tapers towards the apex. The total height from the base to the topmost point is 25.72 m, and it is divided into three sections: (1) base, (2) body, and (3) crown. The pagoda is constructed of unreinforced brick masonry with an estimated volume of 1655 m³. With a brick density of ~1800 kg/m³, its mechanical properties include a Young's modulus of around 1000 MPa and a Poisson's ratio of 0.15[24].

Based on previous studies on the dynamic analysis of inverted bell-shaped pagodas[24], the results revealed a dominant fundamental mode shape. Therefore, a higher number of measurements is not optimal and can significantly increase the computational effort for real-time health monitoring. Two accelerometer sensors are installed on the pagoda, as illustrated in Fig. 3. One is at the top of the body part, considering the crown part is significantly smaller in mass compared to the lower parts, and this signal is hence considered as the structural motion. The other sensor is attached to the pagoda base. The sensors are housed in protective enclosures to shield them from harsh environmental conditions such as temperature fluctuations, humidity, and rain. These sensors measure acceleration in three components: two perpendicular horizontal directions and one vertical direction, with an acceleration range of ±2450 cm/s². Aligned with the tangential and radial directions of the pagoda's structure, the sensors enable real-time measurement of the pagoda's acceleration. Data are recorded at a 24-bit resolution and a sampling rate of 100 times per second, with noise levels as low as 0.1 cm/s², making the system a Class A accelerometer[25]. The collected acceleration data are transmitted to cloud-based storage via a local PC station. Additionally, a notification is immediately sent to the system administrator whenever the sensors detect vibrations exceeding the average ambient levels.

The measured acceleration obtained from Ch2, attached to the top of the pagoda's body, contains both the base motion and the pagoda's body motion. Hence, the acceleration obtained from Ch2 is subtracted by the value measured by Ch1 to obtain the relative acceleration of the pagoda's body, which is used in the mathematical expressions explained in "Mathematical formulations".

Ground motions

The dynamic parameters are determined through the analysis of four remote earthquake datasets, each originating from Myanmar[26] as shown in Fig. 4[27]. Three of these earthquakes occurred in proximity, ~300 km west of the pagoda, with a magnitude of about Mb 5. The fourth earthquake was located 200 km northwest of the pagoda, with a magnitude of Mb 4.6. The occurrence dates of all earthquakes are closely clustered, resulting in minimal impact from time-dependent degradation. Figure 4 depicts the measured base accelerations of the pagoda in the north-south (NS) and east-west (EW) directions, represented in both the time and frequency domains

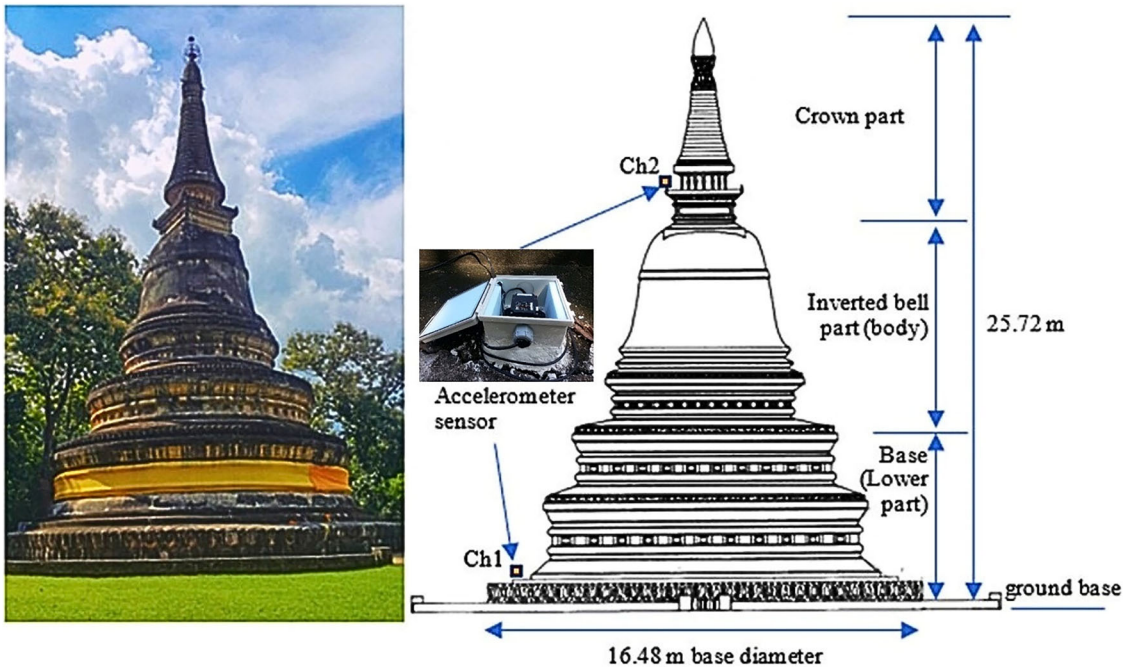

Fig. 3 | Umong Pagoda as the structure under investigation. Photograph of the historic masonry pagoda at Wat Umong, Chiang Mai, Thailand, where the field measurement was conducted. (Source: Authors)

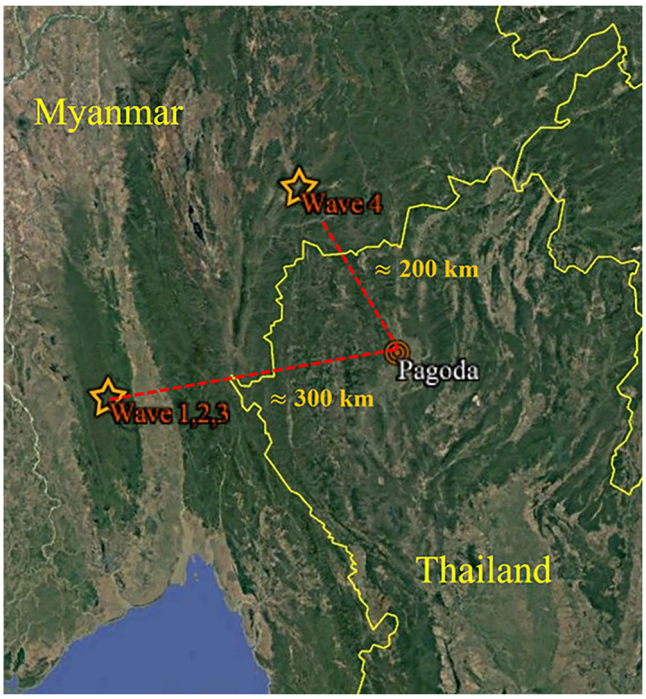

Fig. 4 | Location of earthquake sources and the pagoda. Map showing the spatial relationship between seismic sources (orange stars) and the pagoda site (red circle) using data from Google Earth [27].

of seismic wave 1. In this study, due to the low amplitude of the earthquake waves exciting the pagoda's base, an extended 120-s duration is ensured to cover the vibration range, and a Butterworth filter is applied to reduce the background noise[28]. To increase the number of analytical results with limited waves, 120 s of each wave are fragmented into 12 segments of each 10-s wave. Table 2 provides information on the seismic waves used in this study. The peak base acceleration is between 0.153–0.371 cm/s^2, and the main frequency from the frequency domain analysis is about 0.15–2.53 Hz.

Probabilistic assessment

The probabilistic assessment procedure is employed to perform the uncertainty assessment[29,30] of the dynamic properties of the Umong Pagoda structure subjected to earthquake and seismic hazards. This evaluation is based on the observed time series of acceleration signals obtained from the structural health monitoring system. The dynamic properties, including the damping ratio (ζ) and natural frequency (f), are derived from inverse analysis to facilitate this probabilistic assessment. Various probabilistic models were fitted to the dynamic properties of damping ratio (ζ) and natural frequency (f). Subsequently, the log-normal distribution was identified as the most appropriate model for both the damping ratio and natural frequency. The formulation of the Probability Density Function (PDF) and Cumulative Density Function (CDF) of the log-normal distribution is presented in Eqs. (17) and (18), where μ and σ are the mean value and standard deviation, respectively.

$$\text{PDF}: \quad f(x) = \frac{1}{x\sigma\sqrt{2\pi}} \exp\left[-\frac{(\ln x-\mu)^2}{2\sigma^2}\right] \quad \text{for} \quad x>0 \tag{17}$$

$$\text{CDF}: \quad F(x) = \frac{1}{\sigma\sqrt{2\pi}} \int_0^x \frac{1}{\varepsilon} \exp\left[-\frac{(\ln x-\mu)^2}{2\sigma^2}\right] d\varepsilon \quad \text{for} \quad x>0 \tag{18}$$

Coefficient of determination

The coefficient of determination, R^2, is utilized to assess the goodness of fit between the dynamic properties derived from the inverse analysis. It serves as a statistical measure that quantifies the extent to which the regression line accurately represents the observed data, which is critical for both predictive modeling and hypothesis testing[7,31]. In this study, the earthquake's directionality was considered by incorporating its azimuth in both the North-South (NS) and East-West (EW) directions. Consequently, the coefficient of determination, R^2, was employed to evaluate the goodness of fit of the probability distribution function (PDF) obtained from the probabilistic assessment of the critical damping ratio and natural frequencies in the NS and EW directions. The formulation of the coefficient of

Table 2 | Seismic waves of input ground motion

Wave	Date	Location	Magnitude (mb)	Depth (km)	Distance (km)	Peak base acceleration (cm/s²)		Main frequency (Hz)	
						NS	EW	NS	EW
1	March 17, 2018	18.385°N 96.151°E	5.1	19.1	300	0.159	0.269	0.20	2.53
2	April 20, 2018	18.322°N 96.160°E	5.0	17.1	300	0.153	0.156	0.15	0.16
3	June 17, 2018	18.275°N 96.070°E	5.0	10.0	306	0.181	0.271	0.34	2.28
4	July 1, 2018	20.259°N 97.911°E	4.6	10.0	200	0.362	0.371	0.18	0.29

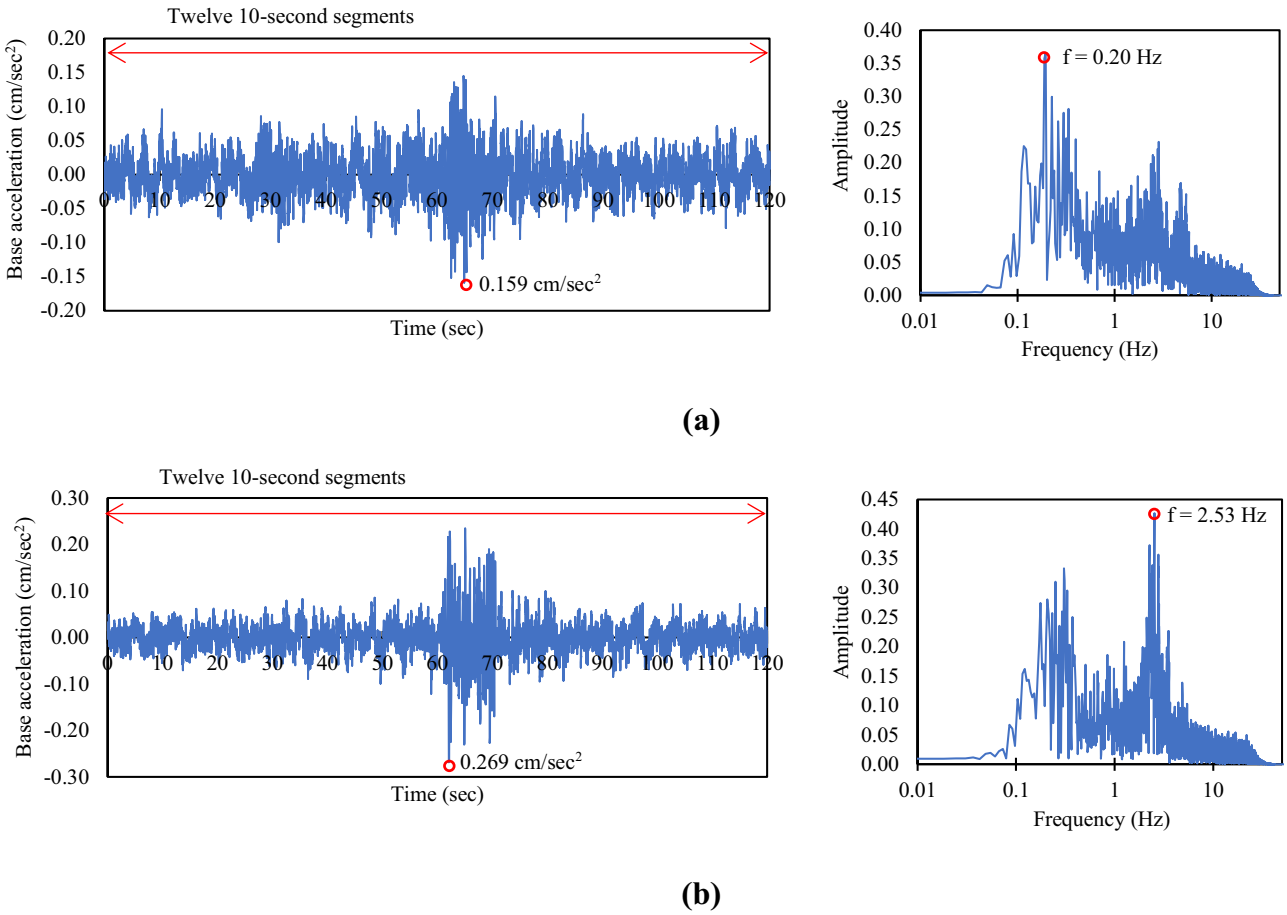

Fig. 5 | Filtered acceleration signals at the base of the pagoda. Filtered acceleration recorded at the base of the pagoda during seismic wave 1: (**a**) North-South direction, (**b**) East-West direction. The Fourier amplitude of acceleration signal is also shown.

determination, R^2, is delineated in Eq. (19).

$$R^2 = 1 - \frac{Sum\ squared\ regression(SSR)}{total\ sum\ of\ squared(SST)} \tag{19}$$

where sum squared regression (SSR) is $\sum (y_i - \hat{y}_i)^2$ and total sum of squared (SST) is $\sum (y_i - \bar{y})^2$. Equation (19) can be rewritten as given in Eq. (20).

$$R^2 = 1 - \frac{\sum (y_i - \hat{y}_i)^2}{\sum (y_i - \bar{y})^2} \tag{20}$$

where y_i is the calculated actual value from the inverse analysis, and $\hat{y}_i$ is the predicted value from the probabilistic model (Probability Density Function, PDF).

Results

Full recorded waves

The inverse analysis conducted for the dynamic parameters, utilizing the 120-s full record of the four seismic waves, yields the convergence of parameters b_1 and b_2, determined by the criteria outlined in Eq. (14), as illustrated in Fig. 6. Subsequently, these parameters are utilized for the calculation of the dynamic properties ζ and f, utilizing Eqs. (15) and (16). From Fig. 6a, b, the parameter b_2 values result in an averaged natural frequency (f) of 3.56 Hz in the NS direction and 3.64 Hz in the EW direction. The averaged damping ratio (ζ) of 2.3% and 1.7% in the NS and EW directions, respectively, is derived from the converged b_1 (and b_2, from Eq. (15)), as depicted in Figs. 6c, d.

Twelve 10-S segmented seismic records

In each seismic wave, the base acceleration time history is divided into twelve 10-s segmental seismic waves, as seen in Fig. 5 for Wave 1.

Table 3 | Inverse analysis results of twelve segments of Wave 1.

Segmental Wave 1	NS Direction			EW Direction		
	b_1	b_2	Iteration	b_1	b_2	Iteration
1	−0.14	0.98	415	−0.49	−0.01	394
2	NaN	NaN	1000	−0.70	−0.31	292
3	6.17	426.09	172	21.44	324.82	359
4	−0.13	521.11	145	0.64	532.01	398
5	1.40	531.74	201	−0.03	545.46	171
6	0.33	498.90	199	0.58	516.82	154
7	0.33	490.40	148	0.51	521.90	125
8	1.40	511.61	212	0.73	538.45	161
9	8.57	428.74	188	0.16	525.45	659
10	8.81	452.24	259	37.05	608.38	270
11	NaN	NaN	1000	NaN	NaN	1000
12	0.06	−0.02	237	1.69	−0.65	187

NaN Not a Number, represents divergence or undefined numeric results, such as the outcome of 0/0 or an infinity value.

Consequently, one fully recorded wave used in the inverse analysis yields twelve results. However, some results from all twelve segmental waves are "Not a Number, NAN" or defined as not realistic, especially in the beginning and ends segments, and those of values are disregarded (too low/too high values). Table 3 presents the results from the segmental inverse analysis of Wave 1. The analysis results of Segments 5–8 are utilized to define the probabilistic dynamic properties. The selection of these segments is based on the values of the damping ratio falling between 0.5 and 10%, which represents the typical damping range of buildings[21]. The results of the four waves, excluding the anomalous values, are shown in Table 4. Figure 6 display the distribution and skewness of the results. The averaged damping ratio stands at 3.2% and 2.3% in the NS and EW directions, respectively, each exhibiting a standard deviation of 2.4%. In terms of natural frequency, the NS and EW directions yield values of 3.60 Hz and 3.64 Hz, respectively, with standard deviations of 0.09 and 0.07, respectively. The coefficient of variation (COV) is used to measure the relative dispersion of events for dynamic parameters of critical damping ratio and natural frequency. It is equal to the ratio between the standard deviation and the mean, as shown in Table 4.

Additionally, the research concentrates on a comprehensive exploration of critical damping ratios and natural frequencies in both the NS and EW directions. This aims to carefully evaluate the uncertainty surrounding the dynamic properties of a Masonry Pagoda. Various probability distribution functions, encompassing the Normal, Log-normal, Weibull, exponential, and Grammar distributions, etc., among others, are thoroughly scrutinized using the maximum likelihood method. The distribution was selected for its ability to capture a sensitive uncertainty factor equally from the mean value. It is well-suited to represent naturally measuring characteristics when boundary values cannot be definitely defined. Consequently, the log-normal distribution is determined to provide the most suitable fit for describing both critical damping ratios and natural frequencies in both NS and EW directions. This can be expressed as follows[32]:

$$\ln x \sim N(\mu, s^2) \tag{21}$$

where variable x represents either critical damping ratio or natural frequency of the structure, μ and s^2 are mean and unbiased variance of natural logarithmic of x, respectively. The symbol $N(\cdot,\cdot)$ is a normal distribution function. These statistical parameters of log-normal distribution related with the mean and unbiased variance of variable x as follows,

$$\mu_x = \exp\left(\mu + \frac{s^2}{2}\right) \tag{22}$$

Table 4 | Inverse analysis results of twelve segments of all 4 waves, excluding the anomalous values

Wave	NS Direction		EW Direction	
	ζ	f (Hz)	ζ	f (Hz)
Wave1-5	0.031	3.67		
Wave1-6	0.007	3.55	0.013	3.62
Wave1-7	0.008	3.52	0.011	3.64
Wave1-8	0.031	3.60	0.016	3.69
Wave2-3	0.016	3.63		
Wave2-4	0.080	3.63		
Wave2-5	0.076	3.66	0.042	3.67
Wave2-6	0.008	3.63	0.007	3.70
Wave2-7	0.015	3.59	0.006	3.73
Wave2-8	0.025	3.72		
Wave3-4	0.005	3.54	0.024	3.60
Wave3-5	0.036	3.84	0.023	3.60
Wave3-6	0.018	3.62	0.010	3.60
Wave3-7	0.014	3.49	0.006	3.58
Wave3-8			0.012	3.57
Wave3-9	0.034	3.62	0.026	3.60
Wave3-10	0.065	3.73	0.014	3.63
Wave3-11	0.043	3.50	0.085	3.72
Wave4-4	0.034	3.44	0.047	3.55
Wave4-5	0.067	3.59	0.010	3.58
Wave4-6	0.017	3.59	0.010	3.67
Wave4-7	0.011	3.49	0.012	3.57
Wave4-8	0.019	3.58		
Wave4-9	0.042	3.55	0.006	3.75
Wave4-10	0.078	3.56	0.084	3.78
Avg	0.032	3.60	0.023	3.64
SD	0.024	0.09	0.024	0.07
COV	0.750	0.025	1.043	0.019
Min	0.005	3.44	0.006	3.55
Max	0.080	3.84	0.085	3.78

$$s_x^2 = \exp(2\mu + 2s^2) - \exp(2\mu + s^2) \tag{23}$$

The dynamic parameters derived from inverse analysis under seismic wave propagation from earthquakes are depicted on probability papers representing the log-normal distribution, as shown in Fig. 7. The values of the log-normal parameters are presented in Table 5.

The coefficient of determination, R^2, is employed to evaluate the goodness of fit between the dynamic properties obtained through inverse analysis and the log-normal distribution function. An R^2 value approaching unity signifies an optimal degree of predictive accuracy. Accordingly, the analysis revealed that, except for the critical damping ratio in both the NS and ES directions, the corresponding dynamic properties yielded R^2 values of 0.975 and 0.934, respectively. Additionally, the R^2 values for the natural frequencies in the NS and ES directions were determined to be 0.981 and 0.942, respectively. Notably, the NS direction exhibited a more pronounced alignment with the log-normal distribution than the WE direction. The specific R^2 values are detailed in Table 4.

Time histories obtained from solved dynamic parameters

The time histories of acceleration in the NS and EW directions, simulated using Newmark's algorithm with average acceleration, are depicted in

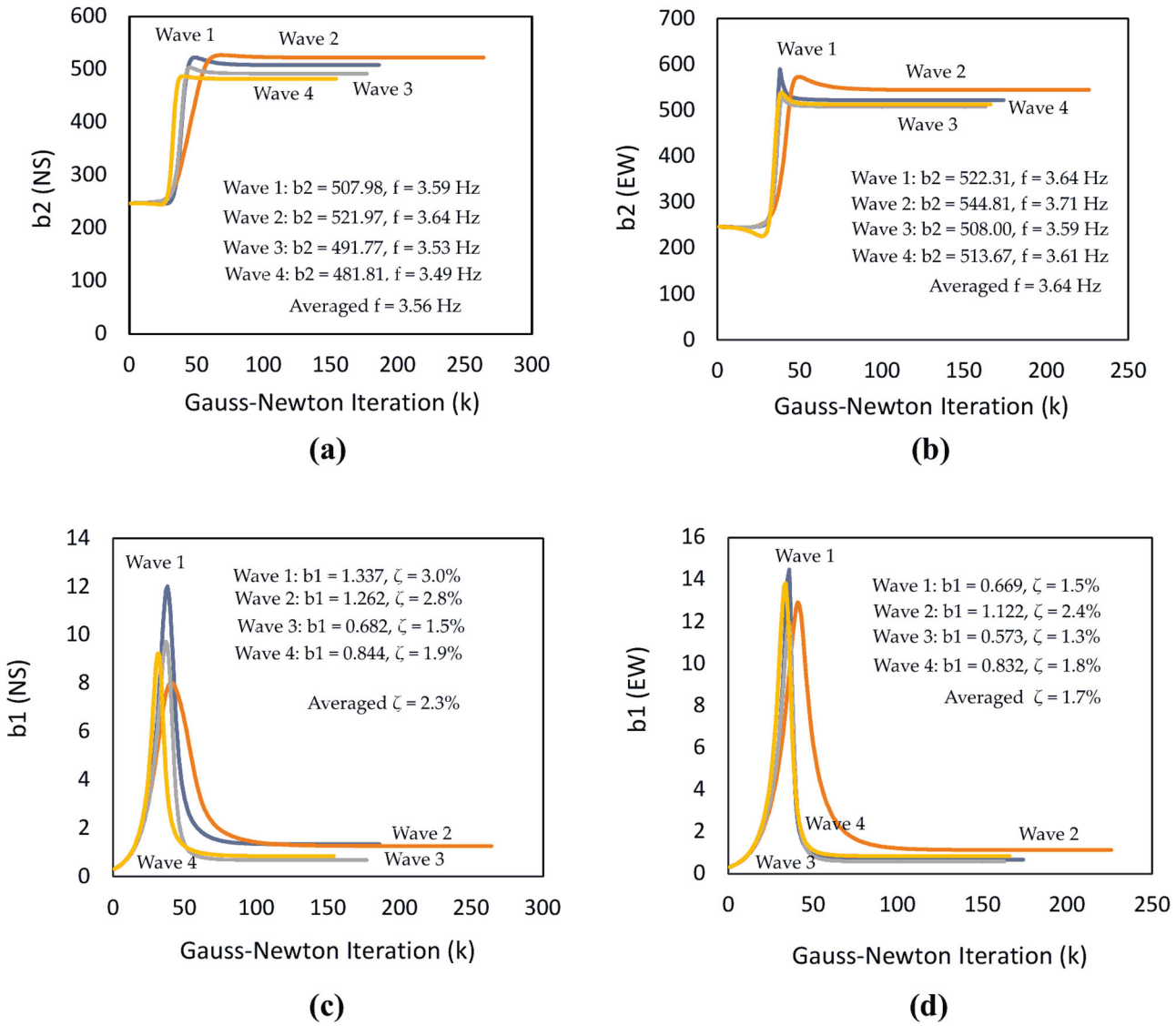

Fig. 6 | Converged dynamic parameters from inverse analysis of full record waves. Each subfigure presents results from four seismic waves. Converged values are derived using the Gauss-Newton algorithm: **a** b_2 and natural frequency f in NS direction, **b** b_2 and f in EW direction, **c** b_1 and damping ratio ζ in NS direction, **d** b_1 and damping ratio ζ in EW direction.

Figs. 8 and 9, respectively. The average dynamic parameters for NS and EW excitations, as derived from Table 3, along with their variations corresponding to two standard deviations (i.e., $\mu - 2s_x$, μ, and $\mu + 2s_x$), were employed in Newmark's algorithm. For the NS direction, illustrated in Fig. 8, the critical damping ratio values are 0.0, 0.032, and 0.08, with corresponding natural frequencies of 3.42, 3.60, and 3.78 Hz. Similarly, for the EW direction, shown in Fig. 9, the critical damping ratio values are 0.0, 0.023, and 0.07, with corresponding natural frequencies of 3.50, 3.64, and 3.78 Hz. It is important to note that any negative damping values resulting from $\mu - 2s_x$ calculations are replaced with zero.

Figures 8 and 9 show that the position of peak acceleration obtained from Newmark's time integration with average dynamic parameters is most corrected. The value of peak acceleration in NS direction is significantly lower than measured value. However, the value of peak acceleration in EW direction is slightly lower than measured value.

Discussion

The comprehensive analysis of the dynamic properties of the Masonry Pagoda under seismic excitations provides significant insights into the structural behavior and inherent characteristics of such heritage structures. The study's findings are discussed in detail below:

The use of the full 120-s seismic records yielded converged parameters b_1 and b_2 which facilitated the accurate calculation of the dynamic properties: the damping ratio (ζ) and the natural frequency (f). The results demonstrated that the Masonry Pagoda exhibits an average natural frequency of 3.56 Hz in the NS direction and 3.64 Hz in the EW direction. These values indicate a relatively uniform stiffness in both directions, differing from the natural frequency determined using Finite Element Method[24] (same pagoda), which was reported as 4.45 Hz in both NS and EW directions. This indicated that the FE method may not fully account for the material deterioration or residual damage accumulated in the structure over its service life. Consequently, this limitation could lead to an overestimate of stiffness and a slightly higher predicted natural frequency, which is crucial for understanding the overall structural integrity under seismic loads.

The damping ratios, 2.3% in the NS direction and 1.7% in the EW direction are within the expected range for such ancient masonry structures. The slightly lower damping ratio in the EW direction suggests a minor discrepancy in energy dissipation characteristics between the two directions.

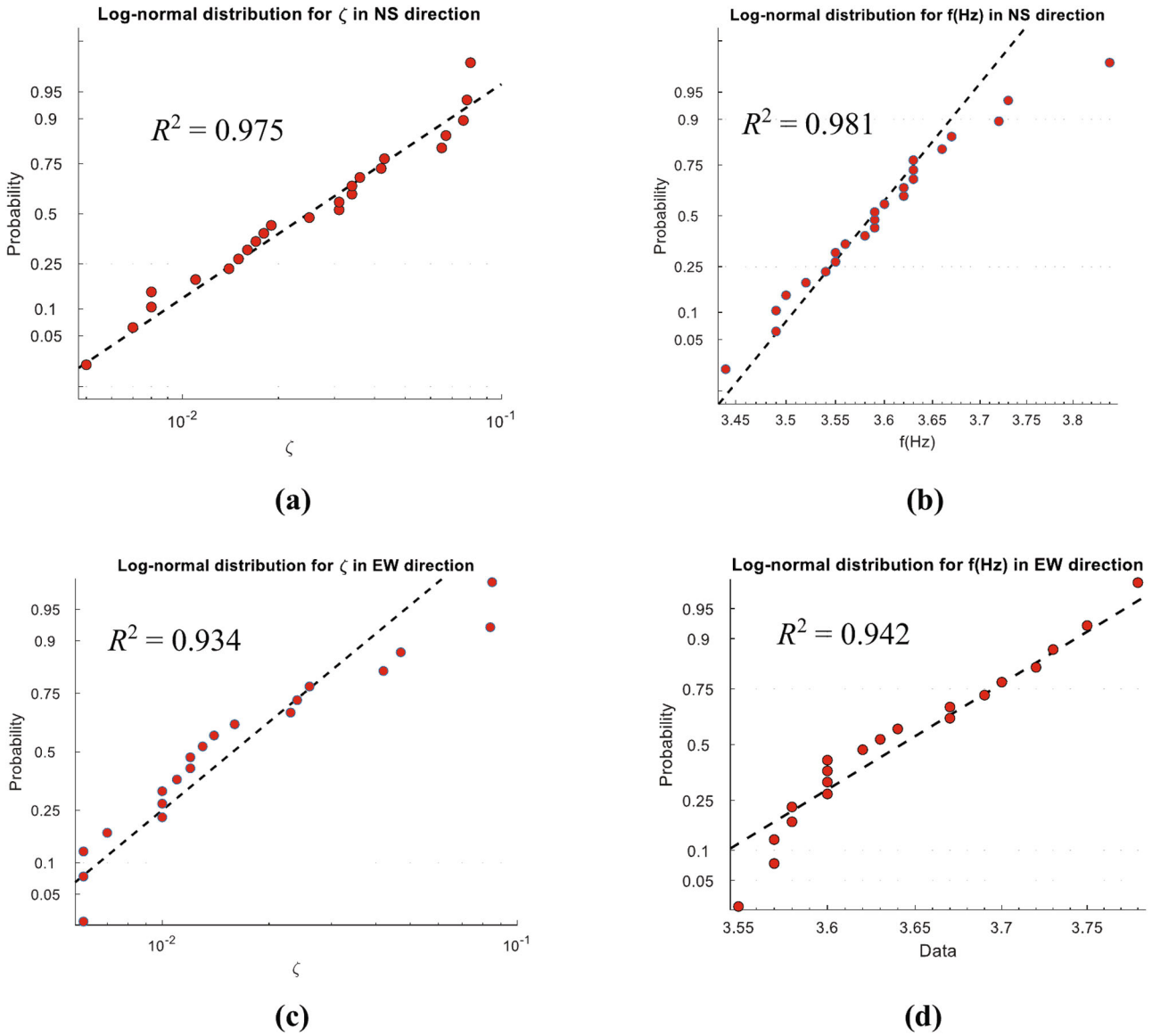

Fig. 7 | Statistical distribution of damping ratio and natural frequency. Probability distributions are fitted to the inverse analysis results. Goodness-of-fit is quantified using R^2 values: **a** ζ in NS direction, **b** f in NS direction, **c** ζ in EW direction, **d** f in EW direction.

Table 5 | Lognormal parameters for the average damping ratio (ζ) and natural frequency (f)

Data	Log-normal Parameters		
	μ	s	R^2
Critical Damping ratio (ζ) in NS direction	−3.717	0.8165	0.975
Natural frequency (f) in NS direction	1.280	0.0242	0.981
Critical Damping ratio (ζ) in EW direction	−4.127	0.8195	0.934
Natural frequency (f) in EW direction	1.292	0.0183	0.942

This could be attributed to material heterogeneity, construction methods, or previous seismic events causing directional variance in the structural properties.

The segmentation of the seismic records into twelve 10-s intervals revealed more granular insights into the dynamic behavior over shorter time frames. Despite some segments yielding non-realistic or NAN results, the majority of the segments provided valuable data. By focusing on segments where the damping ratio fell within the 0.5–10% range, more reliable probabilistic dynamic properties were derived. The averaged damping ratio from the segmented analysis was found to be 3.2% in the NS direction and 2.3% in the EW direction, with standard deviations of 2.4% for both. The corresponding natural frequencies were 3.60 Hz and 3.64 Hz, with standard deviations of 0.09 Hz and 0.07 Hz, respectively. The coefficient of variation (COV) values indicated a moderate level of dispersion, suggesting some variability in the dynamic response, potentially due to factors such as microstructural damage or variations in material properties. For instance, the damping ratio (ζ) estimates exhibited a coefficient of variation (COV) of 0.75 and 1.04 for the NS and EW directions, respectively, reflecting higher uncertainty compared to the natural frequency (f) estimations, which had COV values below 0.03.

The evaluation of various probability distribution functions identified the log-normal distribution as the best fit for describing both critical damping ratios and natural frequencies in the NS and EW directions. The log-normal distribution's parameters were meticulously calculated, providing a robust statistical framework for understanding the variability and reliability of the dynamic properties. The log-normal fit underscores the inherent variability and skewness in the dynamic characteristics, highlighting the need for probabilistic approaches in the seismic assessment of

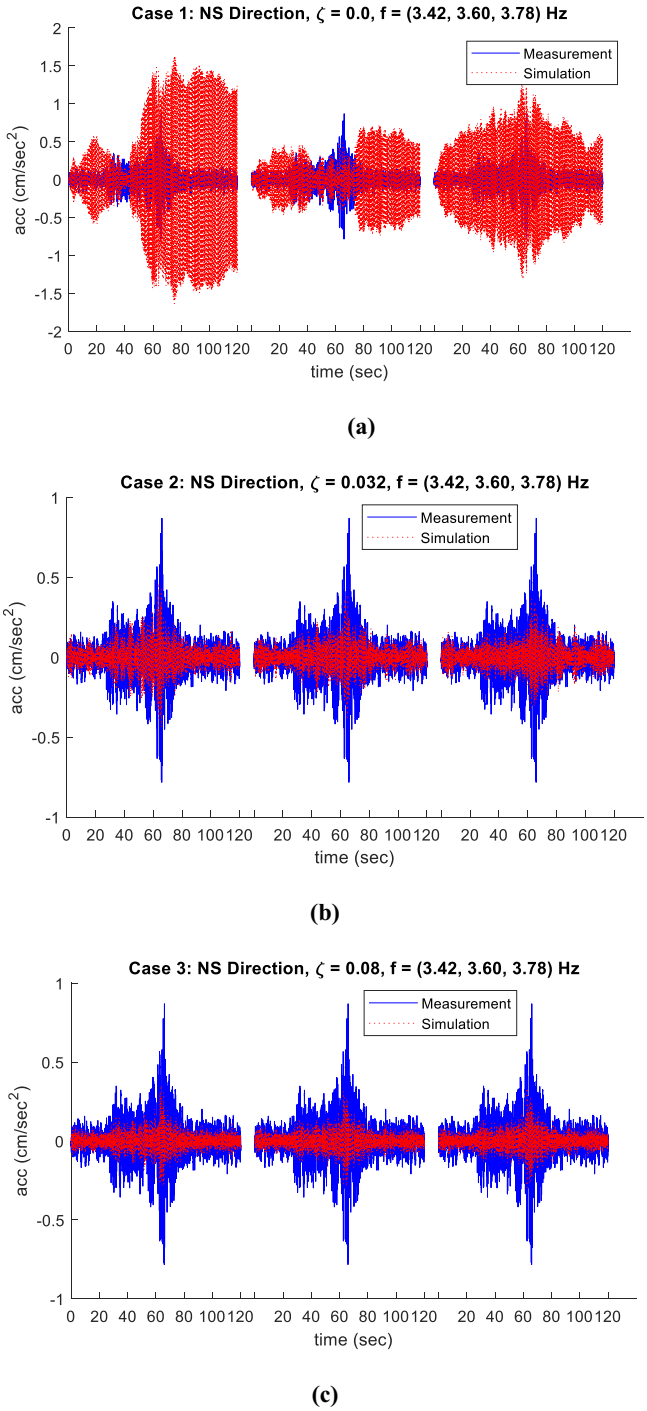

Fig. 8 | Comparison of simulated and measured acceleration in NS direction. Each case uses different combinations of mean and standard deviation of damping ratio and natural frequency in the NS direction: **a** Simulation with $\overline{\zeta} - 2s_{\zeta}$, **b** Simulation with $\overline{\zeta}$, **c** Simulation with $\overline{\zeta} + 2s_{\zeta}$.

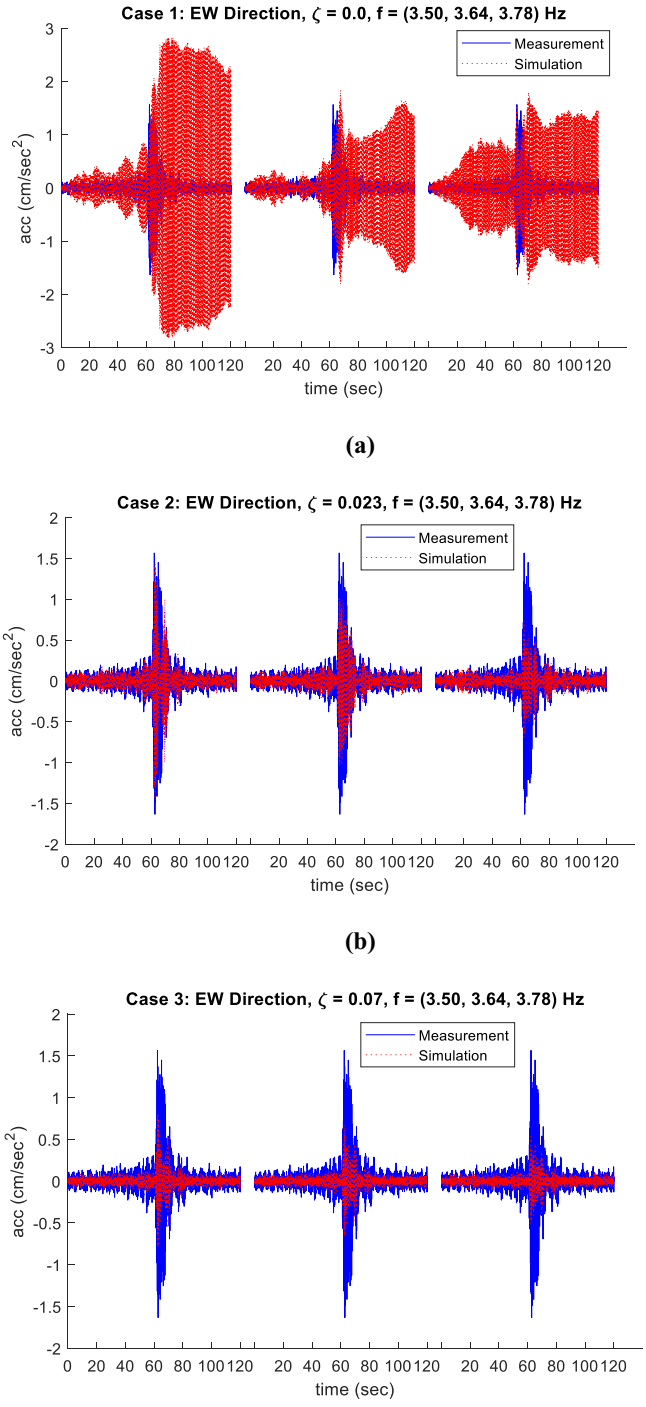

Fig. 9 | Comparison of simulated and measured acceleration in EW direction. Each case uses different combinations of mean and standard deviation of damping ratio and natural frequency in the EW direction: **a** Simulation with $\overline{\zeta} - 2s_{\zeta}$, **b** Simulation with $\overline{\zeta}$, **c** Simulation with $\overline{\zeta} + 2s_{\zeta}$.

heritage structures. This probabilistic understanding is vital for accurate risk assessment and the development of targeted conservation strategies.

The time histories of acceleration generated using Newmark's algorithm with average dynamic parameters and their variations showcased the predictive accuracy of the inverse analysis. In the NS direction, the peak acceleration values obtained were significantly lower than the measured values, indicating potential underestimation of the dynamic response. Conversely, in the EW direction, the peak values were slightly lower, suggesting a closer match between the predicted and actual responses. These discrepancies highlight the complexities involved in accurately modeling the dynamic behavior of historical structures under seismic loads. Factors such as material degradation, complex boundary conditions, and historical alterations can contribute to the observed differences.

The inverted bell shape is a common form of historic Masonry Pagodas in Southeast Asia. Therefore, the results and procedure of this study can be applied to several other pagodas. The findings have significant implications

for the seismic assessment and conservation of long-standing historical heritage structures with uncertain dynamic properties. Structural integrity uncertainties, whether due to degradation over the structure's service life or potential defects during construction, can influence its dynamic properties and the mode shapes. This study, along with several others[11,12,14,15], demonstrates that ambient vibration test serves as an effective method for accurately identifying the actual response of such structures under their actual service conditions. Accurately determining dynamic properties is crucial for developing effective seismic retrofitting strategies that preserve both structural integrity and historical value. The probabilistic approach adopted in this study provides a more comprehensive understanding of dynamic behavior by accounting for inherent uncertainties. This approach can inform more resilient design interventions, ensuring the long-term preservation of heritage structures in seismically active regions.

To address concerns regarding the simplification of the historical pagoda structure as a single-degree-of-freedom (SDOF) system, authors note that this approach is widely adopted for low-amplitude seismic excitation analyses of structures exhibiting a dominant fundamental vibrational mode. Previous studies of inverted bell-shaped pagodas[24] have shown that the fundamental mode governs the dynamic response under such conditions. Consequently, while multi-degree-of-freedom models may capture additional complexities, the SDOF assumption adequately represents the essential dynamic behavior for the purposes of this study. This approach ensures computational efficiency while maintaining analytical robustness, especially for heritage structures with limited input data.

While the proposed inverse analysis method provides valuable insights, it is important to acknowledge its limitations. The SDOF assumption simplifies the structural dynamics, potentially overlooking higher-order mode contributions that may become significant under stronger seismic excitations. Material properties, such as the damping coefficient and Young's modulus, are assumed to be uniform based on literature values[24], introducing potential inaccuracies due to inherent heterogeneities in aged masonry structures. Future studies could address these limitations by incorporating higher-fidelity models and broader datasets.

Data availability

The datasets and codes used and/or analyzed during the current study are available from the corresponding author upon reasonable request.

Code availability

The datasets and codes used and/or analyzed during the current study are available from the corresponding author on reasonable request.

Received: 19 October 2024; Accepted: 25 April 2025;
Published online: 09 May 2025

References

1. Ketsap, A., Hansapinyo, C., Kronprasert, N. & Limkatanyu, S. Uncertainty and fuzzy decisions in earthquake risk evaluation of buildings. *Eng. J.* **27**, 89–105, https://doi.org/10.4186/ej.2019.23.5.89 (2019).
2. Saicheur, K. & Hansapinyo, C. Seismic loss estimation and reduction after structural rehabilitation in Chiang Rai city. *Walailak J. Sci. Technol.* **14**, 485–499 (2017).
3. Saicheur, K. & Hansapinyo, C. Structural repair prioritization of buildings damaged after earthquake using fuzzy logic model. *J. Disaster Res.* **11**, 559–565, https://doi.org/10.20965/jdr.2016.p0559 (2016).
4. Latcharote, P., Hansapinyo, C. & Limkatanyu, S. Seismic building damage prediction from GIS-based building data using Artificial Intelligence system, *Front. Built Environ.* https://doi.org/10.3389/fbuil.2020.576919 (2020).
5. Mase, L. Z., Likitlersuang, S. & Tobita, T. Ground motion parameters and resonance effect during strong earthquake in Northern Thailand. *Geotech. Geol. Eng.* **39**, 2207–2219 (2020).
6. Mase, L. Z., Likitlersuang, S. & Tobita, T. Analysis of seismic ground response caused during strong earthquake in Northern Thailand. *Soil Dyn. Earthq. Eng.* **114**, 113–126, https://doi.org/10.1016/j.soildyn.2018.07.006 (2018).
7. Naess, A. & Moan, T. *Stochastic Dynamics of Marine Structures* (Cambridge University Press, 2012).
8. Kostić, S., Vasović, N., Perc, M., Toljić, M. & Nikolić, D. Stochastic nature of earthquake ground motion. *Phys. A Stat. Mech. Appl.* **392**, 4134–4145, https://doi.org/10.1016/j.physa.2013.04.045 (2013).
9. Zhai, C.-H. & Xie, L.-L. A new approach of selecting real input ground motions for seismic design: the most unfavourable real seismic design ground motions. *Earthq. Eng. Struct. Dyn.* **36**, 1009–1027, https://doi.org/10.1002/eqe.669 (2007).
10. Katsanos, E. I., Sextos, A. G. & Manolis, G. D. Selection of earthquake ground motion records: a state-of-the-art review from a structural engineering perspective. *Soil Dyn. Earthq. Eng.* **30**, 157–169, https://doi.org/10.1016/j.soildyn.2009.10.005 (2010).
11. Compan, V., Pachón, P. & Cámara, M. Ambient vibration testing and dynamic identification of a historical building. Basilica of the Fourteen Holy Helpers (Germany). *Procedia Eng.* **199**, 3392–3397, https://doi.org/10.1016/j.proeng.2017.09.572 (2017).
12. Romero, M. et al. Operational modal analysis: a tool for assessing changes on structural health state of historical constructions after consolidation and reinforcement works—Jura Chapel (Jerez de la Frontera, Spain). *Shock Vib.* **2018**, 1–12, https://doi.org/10.1155/2018/3710419 (2018).
13. Compán, V., Pachon García, P., Cámara, M., Lourenco, P. & Sáez, A. Structural safety assessment of geometrically complex masonry vaults by non-linear analysis. The Chapel of the Würzburg Residence (Germany). *Eng. Struct.* **140**, 1–13 (2017).
14. Salameh, C. et al. Using ambient vibration measurements for risk assessment at an urban scale: From numerical proof of concept to Beirut case study (Lebanon). *Earth Planets Space* **69**, https://doi.org/10.1186/s40623-017-0641-3 (2017).
15. Altunişik, A., Karahasan, O., Okur, F., Kalkan Okur, E. & Özgan, K. Ambient vibration test and modelling of historical timber mosques after restoration. *Proc. Inst. Civ. Eng. - Struct. Build.* **173**, 1–29, https://doi.org/10.1680/jstbu.18.00088 (2020).
16. Buachart, C. et al. Real time vibration measurement and inverse analysis for dynamic properties of an axisymmetric masonry structure. *J. Asian Architecture Build. Eng.* **22**, 2237–2246 (2023).
17. Tantisukhuman, N., Hansapinyo, C., Buachart, C., Miyamoto, M., & Matsushima, M. Earthquake-induced vibration measurement and inverse analysis of bell-shaped Pagoda. In: *Proc. 2nd International Civil Engineering and Architecture Conference*, Singapore, M. Casini, Ed.: Springer Nature Singapore, 342–352 (2023).
18. Klusáček, L., Nečas, R. & Bures, J. Diagnostics of a historical bridge using measuring methods and inverse analysis. *Appl. Mech. Mater.* **764-765**, 1064–1069 (2015).
19. Sinsabvarodom, C., Næss, A., Leira, B. J. & Chai, W. Extreme value estimation of beaufort sea ice dynamics driven by global wind effects. *China Ocean Eng.* **36**, 532–541, https://doi.org/10.1007/s13344-022-0046-3 (2022).
20. Clough, R. W. & Penzien, J. *Dynamics of Structures*. **768** (McGraw-Hill Education (ISE Editions), 1993).
21. Chopra, A. K. *Dynamics of Structures*, 4 ed. 992 (Pearson, 2011)
22. Mitsuhiro, M. & Toshikazu, H. Vibration characteristics of historical masonry buildings based on seismic observation. In: *Proc. 2nd International Conference on Preservation, Maintenance and Rehabilitation of Historic Buildings and Structures*, 789–797 (2015).
23. Singh, N., Ma, L., Yang, H. & Solomonik, E. Comparison of accuracy and scalability of Gauss-Newton and alternating least squares for CANDECOMC/PARAFAC decomposition. *SIAM J. Sci. Comput.* **43**, C290–C311, https://doi.org/10.1137/20M1344561 (2021).

24. Yanathanom, K. Static and Dynamic Behavior under Seismic Loading of Pagodas in Chiang Mai City by Finite Element Method, Master's Thesis, Chiang Mai University, 2010. [Online]. Available: http://cmuir.cmu.ac.th/handle/6653943832/27250
25. Siting Working Group on Instrumentation Installation and Site Metadata of the Advanced National Seismic System Technical Integration Committee, Instrumentation Guidelines for the Advanced National Seismic System, U.S. Geological Survey, Report 2008–1262, 2008. [Online]. Available: https://pubs.usgs.gov/publication/ofr20081262.
26. Pailoplee, S. Mapping of b-value anomalies along the strike-slip fault system on the Thailand–Myanmar border: implications for upcoming earthquakes. *J. Earthq. Tsunami* **11**, 1671001, https://doi.org/10.1142/s1793431116710019 (2017).
27. *Google Earth* https://earth.google.com/ (accessed 8 April 2025).
28. Sriyanto, S., Puhi, A. & Sibuea, C. The performance of Butterworth and Wiener filter for earthquake signal enhancement: a comparative study. *J. Seismol.* **27**, 1–14, https://doi.org/10.1007/s10950-022-10123-7 (2022).
29. Sinsabvarodom, C., Chai, W., Leira, B., Høyland, K. & Naess, A. Uncertainty assessments of structural loading due to first year ice based on the ISO standard by using Monte-Carlo simulation. *Ocean Eng.* 198, https://doi.org/10.1016/j.oceaneng.2020.106935 (2020).
30. Sinsabvarodom, C., Leira, B., Chai, W. & Naess, A. Short-term extreme mooring loads prediction and fatigue damage evaluation for station-keeping trials in ice, *Ocean Engineering*, 242, https://doi.org/10.1016/j.oceaneng.2021.109930 (2021).
31. Sinsabvarodom, C., Leira, B. J., Høyland, K. V., Næss, A. & Chai, W. A generalized ice drift spectrum based on measurements in the Beaufort Sea. *Ocean Eng.* **296**, 116832, https://doi.org/10.1016/j.oceaneng.2024.116832 (2024).
32. Pavlovic, M. Log-normal distribution—a simple explanation. https://towardsdatascience.com/log-normal-distribution-a-simple-explanation-7605864fb67c (accessed 6 June 2024).

Acknowledgements

The authors would like to acknowledge support from Chiang Mai University.

Author contributions

C.H.: Conceptualization, Methodology, Writing – original draft, review & editing, Funding acquisition, Project administration. C.B.: Methodology, Data curation, Writing – review & editing. C.S.: Methodology, Writing, Probabilistic analysis. W.T., W.S., S.L., H.Z., T.G. and V.V.: Supervision, Writing—review & editing. All authors have read and agreed to the final manuscript.

Competing interests

The authors declare no competing interests.

Additional information

Correspondence and requests for materials should be addressed to Chinnapat Buachart.